Available online at www.sciencedirect.com
SCIENCE DIRECT®
Mechanics of Materials 37 (2005) 1–17
MECHANICS OF MATERIALS
www.elsevier.com/locate/mechmat

Longitudinal deformation of fibre reinforced metals: influence of fibre distribution on stiffness and flow stress

Andreas Rossoll *, Benedikt Moser [1], Andreas Mortensen

Laboratory for Mechanical Metallurgy (LMM), École Polytechnique Fédérale de Lausanne (EPFL), CH-1015 Lausanne, Switzerland

Received 7 March 2003; received in revised form 12 November 2003

Abstract

A computational analysis of the longitudinal deformation of continuous fibre reinforced metals is presented. Elastic and elastic–plastic matrix behaviour are considered. Analytical approaches are confronted with finite element analyses (FEA) for varying fibre distributions, ranging from single fibre unit cells to complex cells. Analysis of microfields shows that the main cause for deviation from the equistrain rule of mixtures is a stiffening effect of matrix confinement when surrounded by touching fibres arranged as "rings". Comparison with FEA shows that Hill's [J. Mech. Phys. Solids 12 (1964) 199, 213] bounds, although best possible in terms of volume fraction, are of limited value in so far as Hill's upper bound lies far above any practical limit for a fibre reinforced material, whereas Hill's lower bound loses its bounding property when extended to non-linear behaviour via an incremental scheme. This latter effect can be corrected by changing slightly Hill's derivation in a way that preserves the bounding property. Finally, implications are given for the derivation of in situ matrix flow stress curves from experimental tensile curves on fibre reinforced composites. It is suggested that linear three-point bounds can in practice be used for this purpose.

Keywords: Fibre reinforced composites; Inelastic behaviour; Bounds; Stiffness; Finite element modelling; In situ matrix flow stress

1. Introduction

Assessing the flow stress or stiffness of a unidirectional fibrous material, in which all phases are cylindrical (Hashin, 1983), parallel to the fibres (i.e., in axial loading) is a trivial problem as long as "engineering precision" is sufficient: the equistrain rule-of-mixtures (RoM) applied to the flow stress or stiffness provides adequate precision. The underlying reason is that, when the composite is stressed parallel to aligned fibres, stress and strain are (i) relatively uniform and (ii) far higher along the fibres than in other directions. Hence the average axial stress in each phase roughly equals that which is measured in a tensile bar of the same material taken to the same axial strain ϵ as the composite, i.e.,

$$\sigma_c = V_1\sigma_1 + V_2\sigma_2 \tag{1}$$

with the corollary that, for elastic deformation:

$$E_c = V_1E_1 + V_2E_2 \tag{2}$$

* Corresponding author.
E-mail address: andreas.rossoll@epfl.ch (A. Rossoll).
URL: http://lmm.epfl.ch
[1] Present address: Department of Materials Science, MIT, Cambridge, MA 02139, USA.

0167-6636/$ - see front matter © 2004 Elsevier Ltd. All rights reserved.
doi:10.1016/j.mechmat.2003.12.001

where E denotes Young's modulus, V the volume fraction, and subscripts c, 1 and 2 stand for the composite, Phase 1 and Phase 2, respectively. Eq. (1) and its corollary Eq. (2), adapted when necessary to account for the presence of residual stress in each phase (due for example to thermal contraction mismatch between the phases, see, e.g., de Silva and Chadwick, 1969; Garmong, 1974; Tyson, 1975), are widely known to provide good descriptors of longitudinal composite deformation.

Occasionally, there may arise the need to obtain better precision in linking the longitudinal flow stress of composites with that of its phase constituents. One instance is found with the inverse problem, namely extracting individual phase flow properties from the measured composite stress–strain curve. This has for example been done with fibre reinforced metals to expose size effects in metal plasticity (Kelly and Lilholt, 1969; Isaacs and Mortensen, 1992; Bystricky et al., 1999). This inverse problem is of interest because, with fibre reinforced metals stressed along their axis, phase stresses are relatively uniform in both elastic and elastoplastic deformation (Hill, 1964a,b; Mulhern et al., 1967; Dvorak, 1991; Brockenbrough and Suresh, 1990; Brockenbrough et al., 1991; Böhm et al., 1993; Böhm and Rammerstorfer, 1994). In essentially all other configurations (transversely stressed or laminated fibrous composites, short-fibre or particulate composites...) the matrix stress and strain distributions are highly non-uniform and triaxial, such that the measured average stress has less fundamental meaning without a fully accurate mechanical model (which itself requires knowledge of the in situ phase properties as its input). The reason why higher precision is then required is that, when back-calculating the matrix flow stress from that of a long-fibre composite, the load borne by the generally very stiff fibres far exceeds that which is carried by the matrix. The back-calculated matrix flow stress then results from the subtraction of two far larger numbers (Eq. (1)). Even very minor error in Eq. (1) then causes major uncertainty in the back-calculated matrix flow curve.

Mechanics-related deviations in the composite flow stress or modulus from the rule of mixtures arise from the presence of lateral stresses, themselves due to incompatibility in lateral deformation between the matrix and the reinforcement. In elastic deformation, this is the case whenever the Poisson ratio differs between matrix and fibres: the two phases then exert a mutual constraint on each other that raises the composite stiffness above the value predicted by the RoM, such that:

$$E_{\Delta v} \equiv E_c - (V_1 E_1 + V_2 E_2) \geqslant 0 \tag{3}$$

Hill has derived bounds for the longitudinal stiffness of unidirectional fibrous materials, and hence for $E_{\Delta v}$ (Hill, 1964a):

$$\frac{4V_1V_2(v_1 - v_2)^2}{V_1/k_2 + V_2/k_1 + 1/G_1} \leqslant E_{\Delta v} \leqslant \frac{4V_1V_2(v_1 - v_2)^2}{V_1/k_2 + V_2/k_1 + 1/G_2} \tag{4}$$

where v designates the Poisson ratio, $G = E/(2(1+v))$ designates the shear modulus, $k = E/(2(1+v)(1-2v))$ the plane strain bulk modulus, and the indices 1 and 2 designate the soft and hard phase, respectively. The lower bound corresponds to the longitudinal modulus of an elementary cylindrical composite consisting of a single fibre of the stiffer phase with circular section embedded in a circular cylindrical shell of the more compliant phase. This simple arrangement yields the same result as the composite cylinder assemblage (CCA) proposed by Hashin and Rosen (1964). The upper bound is constructed by inverting the phase properties.

The Hill bounds, although tight in absolute numbers, are relatively slack with regard to the possible error in "back-calculation" of the flow stress of a soft matrix. In particular, it is intuitively clear that the solution for the upper bound is largely above that of any typical (stiff elastic) fibre reinforced composite, since it describes a hard interconnecting matrix with compliant fibres.

More elaborate models can only be constructed by incorporating information on the spatial arrangement of the two phases. Higher order bounds, e.g., Milton (1982), Torquato (1991), Torquato and Lado (1992) and estimates (Torquato, 1998) are constructed by incorporating statistical information on the arrangement of the phases, e.g., on random arrangements of hard fibres in a soft matrix. Three-point bounds are much

tighter than the Hill bounds (which are two-point bounds), but present the inconvenience that real microstructures (e.g., diffusion-bonded monofilament reinforced metals) are not necessarily random, such that these microstructures may yield responses that lie outside these bounds.

Non-linearity of one or both phases, notably matrix plasticity, introduces considerable complications. Hill (1964b) suggested an extension of his linear derivation (Hill, 1964a) to elastic–plastic behaviour, via an approximated yield criterion and flow rule, using incremental plasticity. The principal approximation made by Hill is that the instantaneous moduli are uniform within the elastic–plastic phase. Eqs. (3) and (4) then remain valid, except that the constant values of the moduli are now replaced by instantaneous values (tangent moduli). Young's modulus, E, now becomes the slope of the uniaxial stress–strain curve (strain hardening rate), $\Theta = \partial\sigma/\partial\epsilon$, where σ and ϵ denote the axial matrix stress and strain components, respectively. The (instantaneous) slope of the composite stress–strain curve, $\Theta_c(\epsilon)$, is now given as

$$\Theta_c(\epsilon) = V_1\Theta_1(\epsilon) + V_2\Theta_2(\epsilon) + \Theta_{\Delta v}(\epsilon) \tag{5}$$

$\Theta_c(\epsilon)$ is a constant under the assumptions given above. The bounds are particularly simple if the weak phase is non-hardening and the strong phase is linear elastic:

$$\frac{4V_1V_2(v_1 - v_2)^2}{V_1/k_2 + V_2/k_1 + 1/G_1} \leqslant \Theta_{\Delta v} \leqslant \frac{4V_1V_2(v_1 - v_2)^2}{V_1/k_2 + V_2/k_1 + 1/G_2} \tag{6}$$

Here, the Poisson's ratio of the phase undergoing plastic deformation, v_1 is set to 0.5. The corresponding plane strain bulk modulus, $k_1 = 3K_1/(2(1 + v_1))$ then equals K_1, which is the conventional bulk modulus (i.e., under hydrostatic loading). According to Hill, the shear modulus of the soft phase, G_1, retains its elastic value. Since Hill's analysis was published (Hill, 1964b), numerous, in part more elaborate, schemes have been proposed. Hill (1965) suggested an incremental self-consistent model. Ebert et al. (1968) also propose an incremental approach, but make a micromechanical analysis of the spread of plasticity. Mulhern et al. (1967) include also fibre non-linearity in their analysis. Most other analytical approaches are based on modifications of the Mori–Tanaka mean field scheme (Mori and Tanaka, 1973; Benveniste, 1987). Plasticity may be accounted for via incremental schemes, see e.g., Lagoudas and Gavazzi (1991), or following deformation theory based on secant stiffness, see e.g., Tandon and Weng (1988).

Common to all of these extended mean field approaches is that they use the same approximation as Hill: both the yield criterion and the current (incremental or secant) matrix stiffness are evaluated from average values, with the implication that the spatial variation of the matrix stress state is neglected. Using a mean-value based yield criterion then results in a sudden transition from elastic to plastic behaviour, and an over-estimation of apparent post yield composite stiffness. Secant approaches are somewhat less stiff than incremental approaches, partly it seems because, in the latter, errors are accumulated during the integration with strain.

Improvements can be made in order to diminish some of these shortcomings. For instance, instead of calculating the equivalent stress entering the yield criterion from averaged stresses, it can be computed from distortional energy (Qiu and Weng, 1992; Hu and Weng, 1998) or from statistical theories (Buryachenko, 1996). Such approaches are typically based on secant plasticity or on the use of variational principles (Ponte Castañeda, 1992). These approaches are therefore limited to (roughly) radial load paths, which can be an important drawback because local load paths typically deviate from radial loading in a composite even under imposed global radial loading, and also because global non-radial loading may be important to consider. For instance, thermal loading in the course of composite processing may precede mechanical loading, and cyclic loading and unloading may be of interest (for example to distinguish isotropic and kinematic hardening components in the measured in situ matrix flow stress). The improvement of analytical bounding and estimation methods for non-linear composites is currently an active field of research, see e.g., Ponte Castañeda (1996); Talbot and Willis (1997); Ponte Castañeda (1997); Suquet (1997);

Talbot and Willis (1998); Ponte Castañeda and Suquet (1998); Ponte Castañeda (2002), where attention is being paid notably to an appropriate representation of local field fluctuations. Apart from their limitation to radial loading, another major inconvenience of these models is their unwieldiness in practical application.

In contrast to the above mentioned analytical methods, numerical methods, above all finite element analysis (FEA), are based on the computation of microfields. This necessitates the definition of a distinct microstructure to be analysed: this may be a simple elementary cylindrical composite as in Hill's (1964a) analytical analysis, periodic regular fibre arrangements, or complex cells that represent a repeated "window" of the microstructure. Complex cells of fibre reinforced composites have also been analysed by FEA (Brockenbrough and Suresh, 1990; Brockenbrough et al., 1991; Nakamura and Suresh, 1993; Moulinec and Suquet, 1994, 1998; Yang et al., 2000), as well as various idealized regular fibre arrangements (Böhm et al., 1993; Böhm and Rammerstorfer, 1994).

This study examines, using FEA, the influence of fibre distribution on the (incremental) stiffness and flow stress of fibre composites under axial loading, in a continuum mechanics framework. Our concern is mainly to what extent the fibre distribution influences stress and strain heterogeneity in the matrix. We find limitations to some analytical models that have been proposed, and show how matrix "constraint hardening" (Hill, 1967) acts in regions that are surrounded by regular rings of touching fibres. Finally we draw conclusions from the present numerical simulations towards deriving the matrix in situ flow stress from that of the composite.

2. Analysis

2.1. Fibre arrangements and boundary conditions

In order to examine matrix "constraint hardening" through fibre confinement, and for the purpose of comparison with analytical solutions, several fibre arrangements have been studied. These range from very simple to "realistic" complex cells.

(a) The original Hill single fibre elementary composites, hard fibre in soft shell and vice versa, Fig. 1, were studied at two fibre volume fractions, namely 0.50320 and 0.68517 (referred to in the following as 50% and 68%, respectively). When analytically computed, Hill's arrangements are referred to as "H−" and "H+" for Hill's lower and upper bounds, respectively. The corresponding numerically computed bounds are abbreviated "H−num" and "H+num".

(b) Hexagonal cells, Fig. 2, corresponding to the periodic hexagonal extension of the two Hill cases, were studied at the same fibre volume fractions as

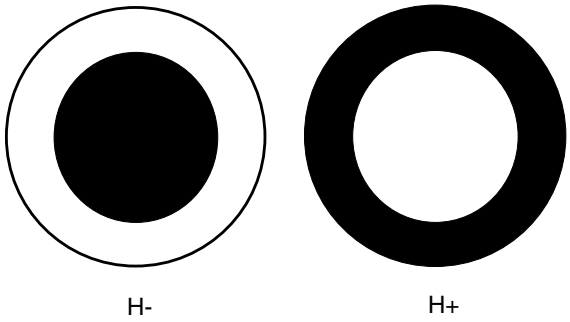

Fig. 1. Hill's single fibre elementary composite. A hard fibre (black) embedded in a soft shell (white) yields Hill's lower bound (H−). A soft fibre (white) embedded in a hard shell (black) yields Hill's upper bound (H+).

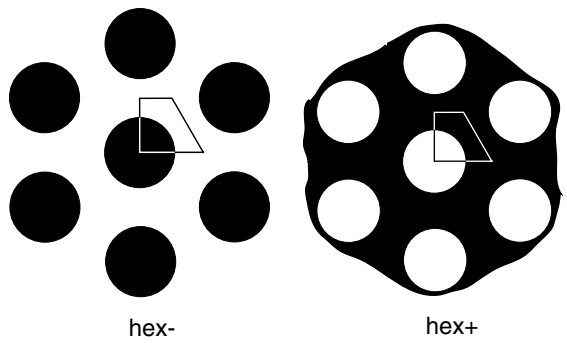

Fig. 2. Periodic hexagonal extension of Hill's elementary composite. The frame designates the unit cell for FEA. Hard fibres (black) embedded in a soft matrix (white) yield a lower bound (hex−). Soft fibres (white) embedded in a hard matrix (black) yield an upper bound (hex+).

the single fibre composites described in (a). Guinovart-Díaz et al. (2001) recently obtained analytical bounds for this arrangement that are very close to Hill's bounds. Here, lower and upper bounds were only computed numerically and are referred to as "hex−" and "hex+".

(c) Complex cells, Fig. 3, were generated with the same fibre volume fractions as the simple cells described above. These feature the following characteristics: (i) The non-dimensional scale parameter δ, defined as the ratio of the cell size L to the size of a characteristic microstructural dimension (Jiang et al., 2001), here the fibre diameter d, equals $L/d \approx 9$. This size of the cell makes it a fairly, but not perfectly, representative (and transverse isotropic) volume element. Stiffness values are thus strictly speaking not "effective" but rather "apparent" (Huet, 1990); however, since loading along the fibre axis does not induce localisation of deformation in planes of intense shear, our "apparent" stiffness values can be expected to be very close to "effective" ones. (ii) The fibre arrangement in the complex cells is such that it allows for periodic boundary conditions (see at the end of this section). (iii) The fibre arrangement is not directly derived from micrographs of an actual composite, since these are never truly periodic; however, it is inspired from images of fibre reinforced aluminium (Isaacs and Mortensen, 1992; Bystricky et al., 1999; Moser et al., 2001). Three fibre arrangements with differing number of fibre contacts were studied for

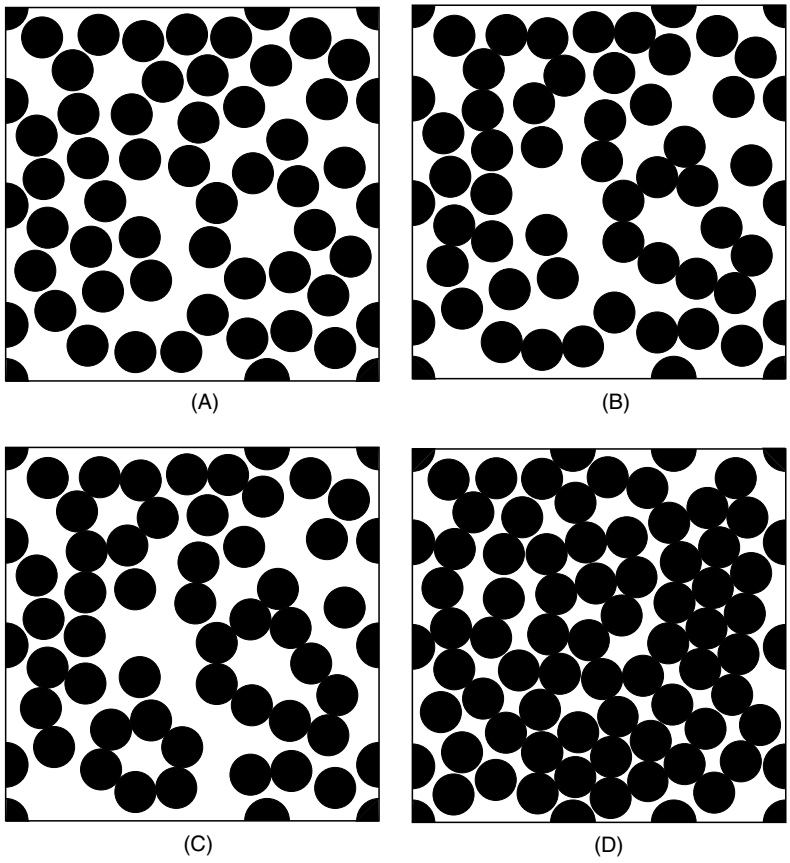

Fig. 3. Complex cells modelled via FEA. The fibre distributions are representative for typical high volume fraction fibre reinforced metals. The arrangements A, B, and C are similar ($V_f \approx 0.50$), except that the number of fibre-to-fibre contacts increases from A to C. D: $V_f \approx 0.68$. See Table 2 for detailed information.

the cell with $V_f \approx 50\%$. These were obtained by varying slightly the position of the fibres and feature either no touching fibres (“A”), some touching fibres (“B”), or “rings” of touching fibres that confine the matrix (“C”). The cell with a fibre volume fraction of roughly 68% is abbreviated “D” and contains several touching fibres with enclosed matrix areas—as expected given the higher fibre packing density.

(d) Matrix confinement through fibre rings is pushed further with “artificial” arrangements (“E1” to “E5”, Fig. 4). In arrangement E1 matrix is only present inside the ring of fibres, whereas in arrangements E2 to E5 matrix is also present between the individual fibre rings. Study of these “artificial” arrangements is largely motivated by the expectation that they yield estimates of upper bounds for composites reinforced with monodispersed fibres.

(e) Finally, two cells were generated that correspond to the percolation limit of monodisperse cylinders in square (“E6”, $V_f = 0.78540$) or hexagonal (“E7”, $V_f = 0.90690$) packing (Fig. 5).

Tables 1–3 summarise main characteristics of all arrangements that were studied. They differ notably in the number of fibre-to-fibre contacts, and the fraction of matrix that is confined by touching fibres. “Artificial” arrangements E2, E3, E6 and E7 are composed of an in-plane network of touching fibres. An almost closed network of fibres is also present in complex cell D (for $V_f \approx 0.68$), where the fraction of matrix that is confined by fibres would exceed 50% by shifting only slightly a few fibres to different positions.

The distribution of fibres in the complex cells is not perfectly random; a check of the lateral deformation components was conducted for the cells with $V_f \approx 0.50$ in order to estimate the extent to which transverse isotropy in respect to the fibre axis is achieved. The maximum difference between the two lateral strain components is a few percent for elastic–plastic matrix behaviour, and smaller by an order of magnitude for an elastic matrix. The deviation from transverse isotropy is thus considered negligible.

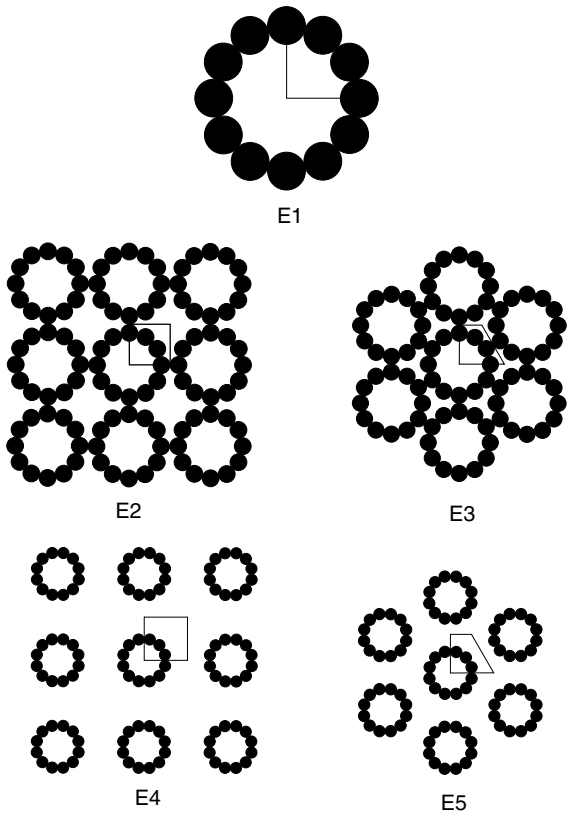

Fig. 4. Artificial arrangements of fibres forming rings. The frame designates the unit cell for FEA. E1: Single ring of 12 fibres confining the matrix. E2: Periodic cubic arrangement of E1. E3: Periodic hexagonal arrangement of E1. E4: Periodic cubic arrangement of E1, but fibre rings are distant. E5: Periodic hexagonal arrangement of E1, but fibre rings are distant. In cells E2–E5 the matrix is both inside the fibre rings as well as in between them.

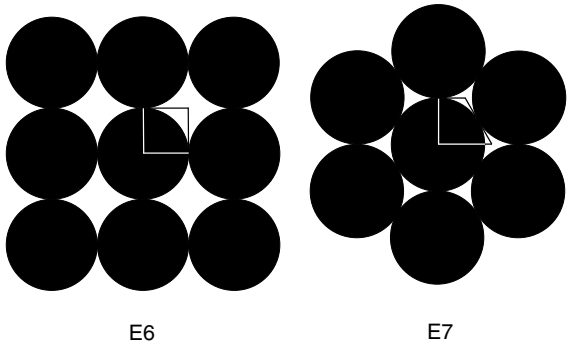

Fig. 5. Cells of fibres at the percolation limit. The frame designates the unit cell for FEA. E6: Cubic. E7: Hexagonal.

Table 1
Characteristics of the simple fibre models

	Abbreviation			
	H−(num)	H+(num)	hex−	hex+
Fibre volume fraction V_f	0.50320/0.68517	0.50320/0.68517	0.50320/0.68517	0.50320/0.68517
Average number of contacts per fibre	0	[a]	0	[a]
Percentage of soft phase that is confined by hard phase [%]	0	100	0	100

[a] Fibre and matrix phase in "reverse" arrangement, i.e., soft "matrix" in hard "fibre" shell.

Table 2
Characteristics of the complex fibre arrangements studied

	Abbreviation			
	A	B	C	D
Fibre volume fraction V_f	0.50320	0.50320	0.50320	0.68517
Number of fibres	52	52	52	71
Number of fibre-to-fibre contacts	0	24	31	84
Percentage of matrix that is confined by hard phase [%]	0	0.1	10.5	28.8

Table 3
Characteristics of the "artificial" fibre arrangements studied

	Abbreviation						
	E1	E2	E3	E4	E5	E6	E7
Fibre volume fraction V_f	0.56456	0.39841	0.46005	0.15784	0.24300	0.78540	0.90690
Average number of contacts per fibre	(2)	2.33	2.5	2	2	4	6
Percentage of matrix that is confined by fibres [%]	100	100 (51.3 inside fibre rings)	100 (65.7 inside fibre rings)	14.8	25.0	100	100

The problem is defined as generalised plane strain with respect to the fibre axis. Loading is applied via a homogeneous deformation parallel to the fibre axis. The in-plane boundary conditions are imposed by the symmetry of the problem with regular arrangements (i.e., all but the complex cells). For the complex cells, periodic boundary conditions were chosen as most suitable.

2.2. Constitutive properties

The stiff phase is assumed isotropic linear elastic with $E_f = 373$ GPa and $\nu_f = 0.235$ for Young's modulus and Poisson's ratio, respectively. These properties correspond to those of continuous alumina Nextel™ 610 fibres manufactured by 3M (Wilson and Visser, 2001; Asmani et al., 2001). Different cases are considered for the (fully isotropic) soft phase, whose properties are roughly inspired by those of pure aluminium: (i) linear elastic with $E_m = 70$ GPa and $\nu_m = 0.345$; (ii) "soft" linear elastic and almost incompressible with $E_m = 7$ MPa and $\nu_m = 0.4999845$ (corresponding to the same bulk modulus as in (i)); this choice is motivated by the fact that it corresponds roughly to an elastic description of the next case; (iii) elastoplastic with elastic properties as in (i), an initial yield stress σ_y of 20 MPa, and a linear isotropic hardening rate $H = \partial\sigma_{\text{flow}}/\partial\epsilon_{\text{pl}}$ of 7 MPa. This very low hardening rate corresponds practically to ideal plasticity. This case is of interest because any metallic matrix can be expected to harden in a manner that is bounded by ideal plasticity and elasticity. J_2 flow theory is assumed.

Table 4
Constitutive properties of the matrix, used as input for the computations

	Designation						
	E [GPa]	v	G [GPa]	K [GPa]	k [GPa]	σ_y [MPa]	H [GPa]
Elastic	70	0.345	(26)	(75.27)	(83.94)	–	–
Soft elastic, almost incompressible	0.007	(0.4999845)	(0.002)	75.27	(75.27)	–	–
Elastic–plastic Hill (Eq. (6))	0.007	0.5	26	75.27	75.27	–	–
Elastic–plastic FEA & MTM	70	0.345	(26)	(75.27)	(83.94)	20	0.007

Brackets ( ) indicate that Young's modulus E, Poisson's ratio v, the shear modulus G, the bulk modulus K and the plane strain bulk modulus k are interdependent. By imposing two independent moduli they can be inferred via the usual relations. σ_y designates the yield strength and $H = \partial\sigma/\partial\epsilon_{\mathrm{pl}}$ the plastic hardening modulus.

In all cases, the strain range of interest is small, typically below 0.5%, because even high-strength ceramic fibres start breaking at this value. Table 4 summarises the constitutive properties of the matrix, as used in analytical as well as in numerical analysis.

2.3. Numerical solution

The boundary value problems defined above were solved with the commercially available FEA package Abaqus/Standard (version 5.8). An updated Lagrangian framework (NLGEOM option in Abaqus) was employed; however, overall strains are small, and comparative computations with a small strain assumption show that resulting differences are negligible. The maximum size of residuals was set to 1.0×10^{-6} of the average force. For further details on the solution method, we refer to HKS (1998).

Twenty fully integrated axisymmetric elements with quadratic interpolation were used for the discretisation of the original Hill geometry (single fibre in shell, Fig. 1). Generalised plane strain elements with quadratic interpolation were employed in the other mesh designs. 300 fully integrated quadrilateral elements were used for the simple hexagonal arrangement cells (Fig. 2); triangular elements were employed for the other cells, with a number ranging from roughly 600 (cell E1, Fig. 5) to over 22,000 for the complex cells (Fig. 3).

A convergence study on the "fibre rings" complex cell C with elastic–plastic behaviour showed a vanishingly small difference between stiffnesses as compared to a much finer mesh (87,000 elements). Differences in the values of average field variables, evaluated at an axial strain of 0.005, between the standard and fine mesh designs are slightly higher but still negligible (Rossoll et al., 2003). Thus it was concluded that the level of discretisation is sufficient.

A perfect interface is assumed between the fibres and the matrix, and there are no voids in the fibres or in the matrix. Contact between fibres was realised as a perfect bonding along a cylinder generator via one common node. This solution does not allow for sliding of one fibre on the other, but allows for a relative rotation between fibres around this common node, such that any forces are transmitted, but only limited moments. For the case studied, i.e., a stronger lateral contraction of the matrix as compared to the fibres and axial tensile loading, contact forces are mostly normal compressive forces that are well handled with this approach.

2.4. Analytical computations

Linear elastic solutions for some analytical models were computed with the COMPCOMP software (Böhm, 1998). The models considered are the rule of mixtures over stiffnesses, the Hill bounds, and three-point bounds (Milton, 1982; Torquato, 1991). The three-point bounds used here consider the case of hard (i.e., non-penetrable) cylinders. Hashin's CCA approach and the Mori–Tanaka mean field ("MTM") scheme correspond to Hill's lower bound.

Incremental elastic–plastic solutions were generated for the Hill (1964a) bounds (Eq. (6)) and for the Mori–Tanaka model. The implementation of

the latter follows Lagoudas and Gavazzi (1991) and makes use of a numerical evaluation of Eshelby's tensor according to Gavazzi and Lagoudas (1990).

3. Results

3.1. Composite flow stress and modulus

Stiffness values E or Θ were computed in FEA from the reaction forces and nodal displacements. These "globally" evaluated values are identical with values evaluated from the averaged stresses and strains. The stiffness values extracted from elastic computation of matrix behaviour are initial values (for zero strain).

Plotted in Fig. 6 are the values of the $E_{\Delta v}$ or $\Theta_{\Delta v}$ terms (from Poisson's ratio mismatch), for the three matrices examined: (a) elastic; (b) soft elastic, nearly uncompressible; (c) elastic–plastic. $E_{\Delta v}$ has been defined in Eq. (3). $\Theta_{\Delta v}$ follows easily from Eq. (3) as

$$\Theta_{\Delta v} = \Theta_c(\epsilon) - V_1\Theta_1(\epsilon) - V_2\Theta_2(\epsilon) \tag{7}$$

The Hill bounds are shown together with three-point bounds (for the elastic cases) or with results from incremental MTM modelling (elastic–plastic matrix), and results of numerical modelling.

For elastic matrix behaviour, the following observations can be made, Fig. 6(a): (i) the Hill bounds are tight and lie close to the RoM solution (the abscissa on the plots); (ii) the numerical computations of the Hill arrangements (H−num, H+num) and of hexagonal unit cells (hex−, hex+) yield practically identical solutions that correspond also to the analytical Hill bounds H− and H+; (iii) the numerical solutions of the complex cells (A–D) lie well within the three-point bounds, with a tendency to approach the upper bound for the higher volume fractions near the random percolation limit (no analytical solutions are available for fibre volume fractions higher than roughly 70%); (iv) the "artificial" arrangements E yield a solution that is well below Hill's upper bound but above the three-point bounds.

Nearly incompressible "soft" elastic matrix behaviour is plotted in Fig. 6(b): (i) the analytical bounds become much larger, with $E_{\Delta v}$ reaching up to almost 5 GPa for Hill's upper bound, whereas the analytical lower bounds fall as expected on the RoM; (ii) the numerically computed simple cells (H+num, H−num, hex−, hex+) still coincide with the analytical bounds; (iii) the complex cells (A–D) also lie on the low side, but still with a tendency to stiffen slightly towards high fibre volume fraction; (iv) again the "artificial" arrangements fall between the Hill bounds, but lie closer to the lower bound as compared to the elastic "hard" matrix case (Fig. 6(a)).

For the elastic–plastic matrix, $\Theta_{\Delta v}$ is plotted in Fig. 6(c) for an imposed nominal strain of 0.1%. As compared to the elastic cases, the following characteristics become apparent: (i) Hill's analytical bounds are much wider than for the "hard" elastic case, but tighter than for the soft elastic/nearly incompressible case. (ii) The numerical upper bound solutions lie a bit below the corresponding analytical bounds; the numerical lower bound solutions now lie well below the analytical bounds and approach the RoM. (iii) The complex cells are also below the analytical lower bounds. (iv) Most of the "artificial" arrangements yield solutions above the analytical lower bound except at lower volume fraction (where fibre rings do not touch).

3.2. Local stress and strain distributions

Fig. 7(a) and (b) depict contour plots of the stress component along the fibre axis, in the fibre and matrix phase, respectively, for complex cell "C" (some fibres confining the matrix), with elastic–plastic matrix properties at an axial strain of 0.005. Lateral contact between fibres clearly influences the stresses in the fibres. Touching fibres carry on average a slightly lower stress than isolated ones; however, the effect is limited. Relatively more important is the confinement of matrix through rings of touching fibres, which creates "islands" of increased stress triaxiality, causing in turn an increase of the axial component of the stress borne by the matrix ("constraint hardening"). Beyond these regions, the stress distribution is fairly uniform, apart from small regions that are compressed by adjacent fibres (black regions).

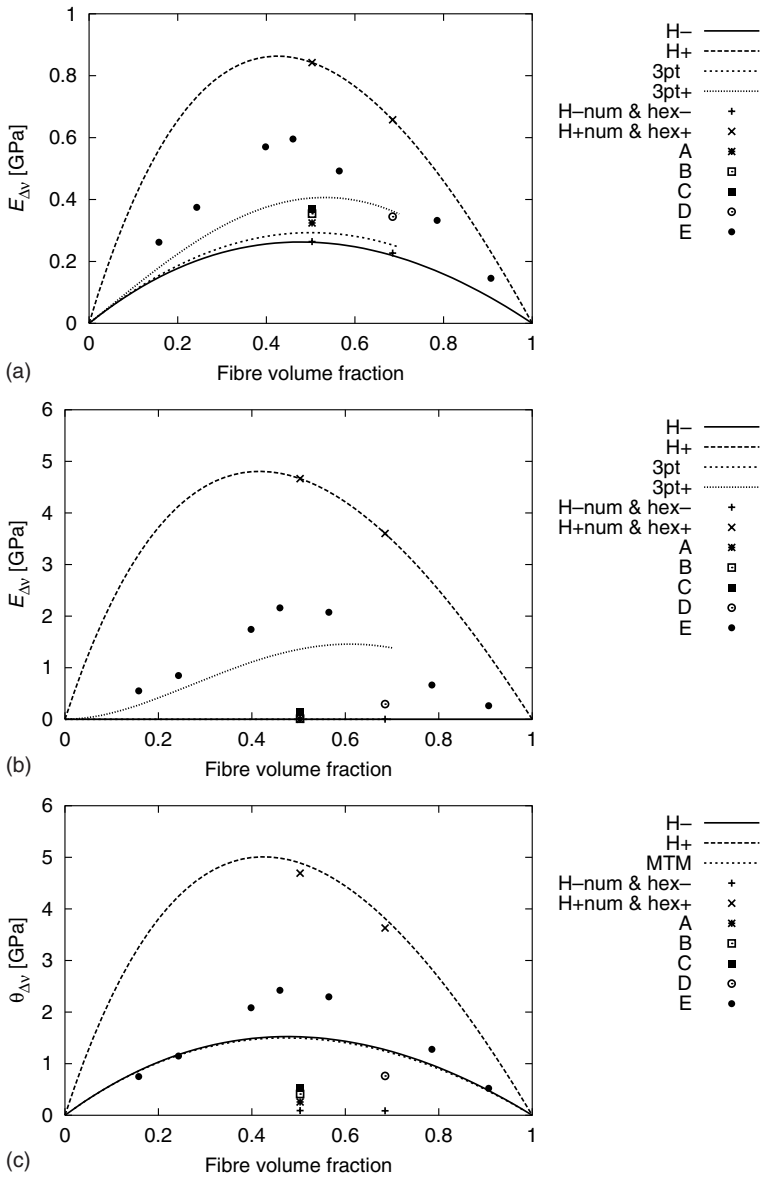

Fig. 6. Composite stiffness computed with different models, for different matrix materials: (a) elastic; (b) soft elastic, nearly incompressible; (c) elastic–plastic. The material properties are specified in the text. The values shown are the contribution to stiffness from lateral contraction mismatch of the two phases $E_{\Delta v}$ (elastic matrix behaviour) or $\theta_{\Delta v}$ (elastic–plastic matrix behaviour). (a,b) refer to zero composite axial strain, (c) to a strain of 1×10^{-3}. H– and H+ stand for Hill's lower and upper analytical bounds; 3pt– and 3pt+ are three-point lower and upper bounds; H±num and hex± stand for numerically computed bounds using Hill's fibre/shell rudimentary composite model (H±num), or a hexagonal periodic fibre arrangement (hex±); A–D stand for complex, E for the "artificial" arrangements shown in Figs. 3 and 4 and whose characteristics are summarised in Tables 2 and 3. MTM stands for the Mori–Tanaka mean field method.

The distribution of the axial stress component borne by the matrix is plotted in the form of an accumulated frequency (corresponding to stress values exceeding the values on the abscissa) in

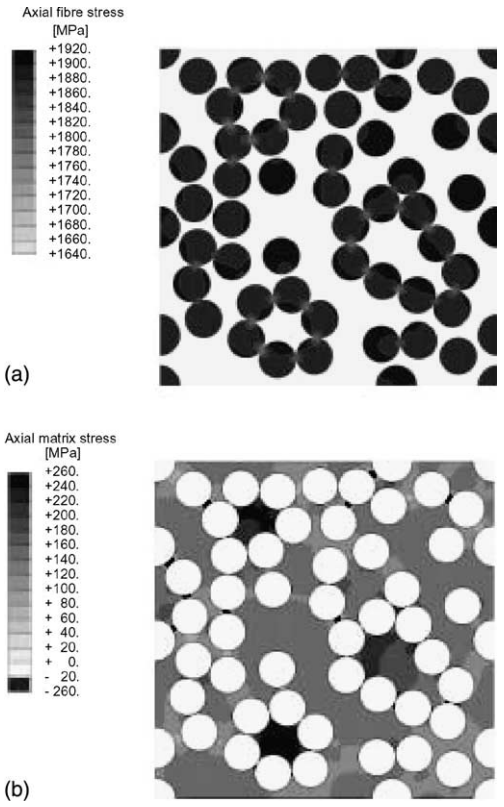

Fig. 7. Contour plot of the stress borne in the axial direction (a) by the fibres, and (b) by the matrix, in cell C ($V_f \approx 0.50$) at an imposed axial strain of 0.005, for an elastic–plastic matrix material.

Figs. 8 and 9, for simple and complex cells. In Fig. 8(a), $V_f \approx 0.50$ and the matrix is elastic; in Fig. 8(b), the matrix is soft elastic, nearly incompressible. In Fig. 9, the matrix is elastic–plastic; in (a) $V_f \approx 0.50$, and in (b) $V_f \approx 0.68$. The following observations apply for all plots: (i) The "hard-fibre-in-soft-shell" (H−num) configuration always exhibits a uniform stress distribution, which corresponds well to the mean value of the hexagonal counterpart (hex−). (ii) Both single fibre and hexagonal upper bound solutions (H+num and hex+) show a constant and identical value of stress borne by the matrix. (iii) Local stress fluctuations are largest in the complex fibre arrangements, as expected. The average matrix stress is always above, but never far, from the H−num case, being a bit further above for higher fibre volume fraction. The average matrix stress in the H+num cell remains above local maxima in all complex cells: the H+num cell is thus not even representative of the upper tail in stress distribution in the complex cells. The more fibres touch, and the more matrix is confined by fibres (compare with Table 3), the larger becomes the upper tail in the stress distribution, whereas the rest of the distribution remains largely unchanged. The influence of matrix confinement seems to be carried over a large portion of the complex cells for elastic hard matrix behaviour, whereas it is more localised for elastic–plastic matrix behaviour.

Similar plots can be obtained for any local field variable. Additional plots and tables containing average field variables and standard deviations can be found in Rossoll et al. (2003). These

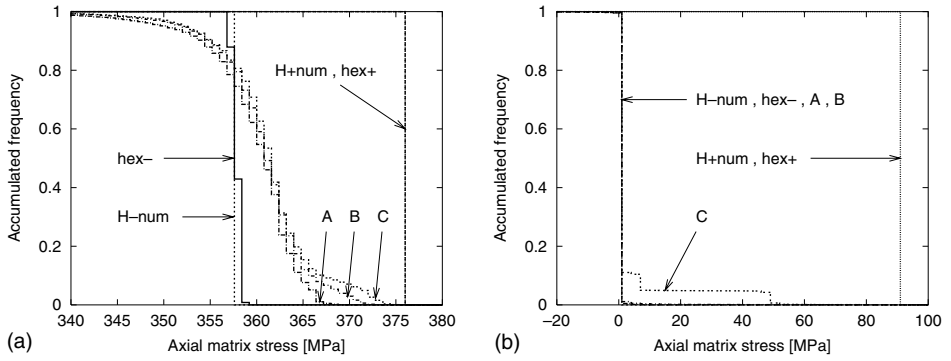

Fig. 8. Plot of the accumulated frequency of the axial stress in the matrix ($V_f \approx 0.50$), at an imposed axial strain of 0.005, (a) for the elastic matrix material, (b) for the soft elastic, nearly incompressible matrix material, showing a comparison of simple and complex arrangements (abbreviations as in Fig. 6).

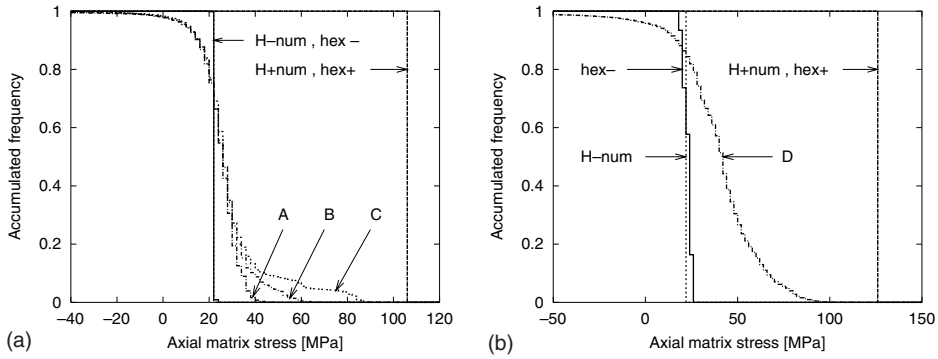

Fig. 9. Plot of the accumulated frequency of the axial stress in the matrix, for the elastic–plastic matrix material, at an imposed axial strain of 0.005, (a) $V_f \approx 0.50$, (b) $V_f \approx 0.68$, showing a comparison of simple and complex arrangements (abbreviations as in Fig. 6).

confirm the trends that are already outlined for the axial stress component borne by the matrix. Field fluctuations are always vanishingly small for upper bound arrangements and fairly small for lower bound arrangements, but may be considerable for the complex cells. "Constraint hardening" is reflected in high values of hydrostatic stress σ_h and of stress triaxiality ($T = \sigma_h/\sigma_{eq}$, where σ_{eq} designates the von Mises equivalent stress), which can be important for the soft elastic and almost incompressible matrix and for the elastic–plastic matrix. In the complex cells, the mean values of all variables always lie much closer to the lower bound solutions than to the upper bound solutions.

3.3. Elastoplastic composite deformation

The described local fluctuation of field variables occurs also with time (i.e. with loading) and may be non-linear, e.g., if elastic–plastic behaviour is considered. The evolution of the volume-averaged axial matrix stress with strain is plotted in Fig. 10(a), for elastic–plastic behaviour. Corresponding to variations of the term $\Theta_{\Delta v}$ across the different models (Fig. 6(c)), the matrix hardening rate due to constraint differs strongly, from a mere 0.3 GPa for the numerical lower bound arrangement, via values around 1 GPa for the complex cells and some 5 GPa for the incremental Mori–Tanaka scheme, to over 17 GPa for the numerical upper

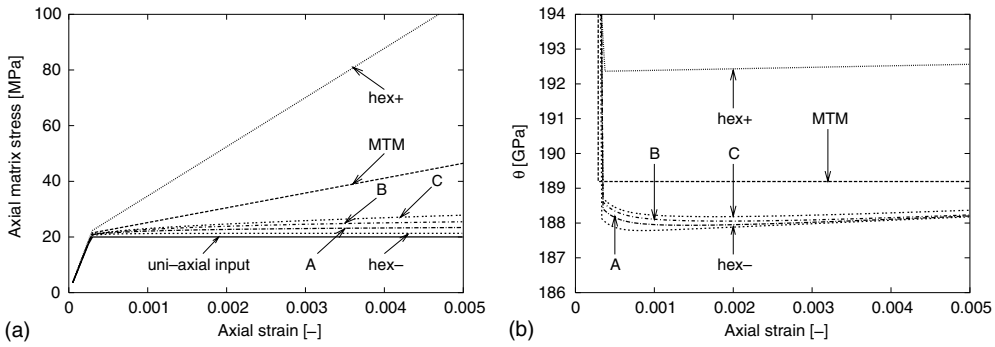

Fig. 10. (a) Evolution with axial strain of the average axial stress borne by the matrix (elastic–plastic matrix, $V_f \approx 0.50$). Predictions of different models. Abbreviations as in Fig. 6. The slopes describing the average "constraint hardening" rates are, from the uppermost curve (hex+) downwards, 17,660, 5319, 1447, 1000, 596 and 268 MPa, respectively. (b) Evolution of the overall composite tangent stiffness in the plastic regime of deformation ($V_f \approx 0.50$), computed with different models.

bound solution. The prediction of the yield stress, on the other hand, is almost identical for all models.

The differences in matrix "constraint hardening" rates are also reflected in differences of the overall composite stiffness, as plotted in Fig. 10(b) for the plastic regime of deformation. Only the (semi-)analytical MTM model yields a constant value of $\Theta(\epsilon)$, whereas all numerical solutions clearly show a variation of the composite stiffness with strain. The transition from elastic to plastic behaviour is not instantaneous but occurs over a finite strain interval over which $\Theta_{\Delta v}(\epsilon)$ varies significantly. This is evidently due to the local field fluctuations, and the inhomogeneous and non-proportional stress distribution during the transition from elastic to elastoplastic deformation regimes. Past this transient, above about 0.1% or 0.2% strain, $\Theta(\epsilon)$ becomes far more constant. The existence of such a transient between elastic and fully plastic regimes was also found in earlier work on particulate composites with elastic-perfectly plastic or Ramberg–Osgood matrices (Bao et al., 1991).

A closer look at the evolution of stiffness with strain is obtained by plotting only the $\Theta_{\Delta v}(\epsilon)$ term. It is then found that this terms evolves with strain, also for linear phase behaviour, as a consequence of the influence of differential lateral contraction on the instantaneous phase volume fraction (the two phases contract laterally at different rates). This effect is, however, of second order and can be neglected. A more detailed analysis can be found in Rossoll et al. (2003).

4. Discussion

4.1. Geometrical effects

The simulations show to what degree the global longitudinal stiffness of a long-fibre reinforced composite can be influenced by the local arrangement of fibres (Fig. 6). Whereas a periodic hexagonal arrangement of fibres of each phase yields global and local solutions that are indeed very close to Hill's elementary single fibre composite bounds, typical stiff fibre composites have stiffnesses that vary over a significantly smaller range. "Realistic" fibre arrangements are somewhat stiffer than the lower bound; still, the composites remain far more compliant than the upper bound. Even "artificial" fibre arrangements in the form of regular rings produce a composite stiffness that traverses only half the distance that separates soft-shell/hard-fibre from hard-shell/soft-fibre arrangements. The upper bound is thus far too high for fibre composites.

Deviations in the modulus of fibre composites from Hill's lower bound are chiefly due to matrix confinement ("constraint hardening") where it is surrounded by rings of contacting fibres. When the fibre ring is not circular, the level of matrix triaxiality attained is somewhat lower, Fig. 7, seemingly because deformation of the ring can relieve some of the lateral strain mismatch.

The correlation between such "constraint hardening" and the amount of matrix that is confined by rings of fibres, or the number of fibre-to-fibre contacts, can easily be verified. Compare the number of fibre-to-fibre contacts, and the percentage of matrix that is confined by fibres, both given in Tables 1–3, with the stiffness values plotted in Fig. 6. This observation also holds for elastoplastic matrix behaviour: the stiffness increase $\Theta_{\Delta v}$ over the RoM equals, for the elastic–plastic matrix and at a longitudinal strain of 0.1%, 258 (cell A), 411 (cell B), 528 (cell C), and 762 (cell D) MPa. The same qualitative correlations between microstructure and stiffness can also be made for the simple cells and the "artificial" fibre arrangements. Confined matrix regions are also responsible for the long upper tail of the matrix stress distribution plotted in Figs. 8 and 9, which extends with increasing importance from cell A to D. Notably stress triaxiality is sensitive to fibre arrangement (see the tables in Rossoll et al., 2003).

4.2. Elastic–plastic soft phase

Our calculations confirm that Hill's linear elastic bounds are the best possible for linear fibrous materials in terms of volume fraction alone (which of course comes as no surprise). Without exception, all numerical results lie within, or on, these bounds (Fig. 6(a)). This is also true for soft

elastic, almost incompressible, matrix behaviour (Fig. 6(b)). Three-point bounds are much tighter and enclose all solutions derived for the "realistic" complex cells, which eloquently demonstrates their utility. "Artificial" cells may, on the other hand, lie above the three-point upper bound.

Hill's incremental elastic–plastic bounds (Hill, 1964b) are on the other hand too stiff. The lower bound loses its bounding property: some of the numerical solutions, notably those obtained for the complex cells, lie well below Hill's lower bound and approach the RoM solution (Fig. 6(c)). The incremental Mori–Tanaka model yields a solution very close to Hill's lower bound, and is thus also not a very good descriptor of the composite apparent rate of work hardening.

This overly stiff behaviour of Hill's elastic–plastic bounds does not seem to be due to the incremental approach or assumptions taken with regard to strain and stress distribution. Rather, it is due to assumptions concerning the values used for the different matrix stiffness moduli. Indeed, whereas it is reasonable to attribute a value close to 0.5 to Poisson's ratio, a value close to zero for Young's modulus (for a non-hardening matrix) and the elastic value to the bulk modulus, the tangent shear modulus of an elastic–plastic material cannot remain at its elastic value, as done in the expression given by Hill (1964b). Instead, preserving the elastic value only for the bulk modulus together with the common relations between all the moduli (as for the soft elastic, almost incompressible matrix material in this study, see Table 4) yields approximate bounds that can be used for elastic–plastic matrix behaviour.

This is illustrated in Fig. 11, where the analytical solutions obtained for the soft elastic, nearly incompressible matrix from Fig. 6(b) are combined with the numerical solutions for an elastic–plastic matrix from Fig. 6(c). Hill's linear bounds now work very well, and the linear three-point bounds also bracket well the complex cells solutions (random composites). In addition, the upper bound fits the numerical solutions better than does Hill's original incremental approach (Fig. 6(c)).

Although no rigorous proof is given here and although the strain dependence of $\Theta_{\Delta v}(\epsilon)$ is neglected, these "modified Hill" linear bounds thus seem usable in practice for elastic–plastic matrix behaviour. Finally, for typical random microstructures, the linear three-point bounds for non-hardening matrix are fairly narrow while still bounding the numerical solutions. This suggests that they constitute practically useful bounds for $\Theta_{\Delta v}$ even with elastic–plastic matrix composites.

4.3. Implications for the "back-calculation" of in situ matrix properties

From Eq. (7) it follows that the matrix in situ uniaxial flow stress can be derived from

$$\sigma_m^{\text{flow}} = \frac{\sigma_c(\epsilon) - (V_f E_f + \Theta_{\Delta v}) \cdot \epsilon}{1 - V_f} \tag{8}$$

if the strain dependencies of V_f and $\Theta_{\Delta v}$ are neglected. Assuming that the (initial) fibre volume

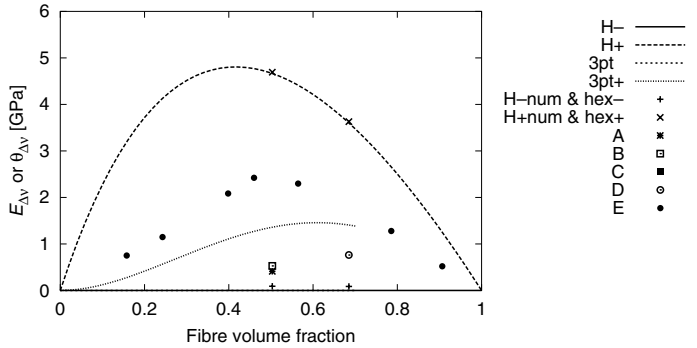

Fig. 11. Comparison of analytical bounds for soft elastic, nearly incompressible behaviour, with FEA solutions for elastic–plastic behaviour. The analytical solutions are taken from Fig. 6(b), the numerical ones from Fig. 6(c).

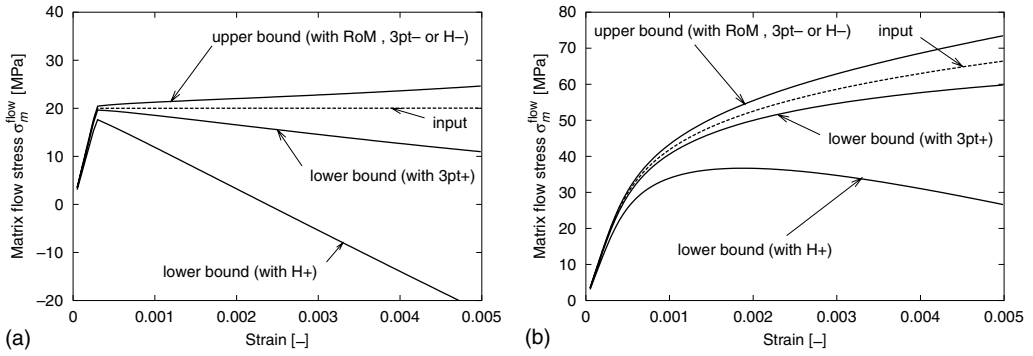

Fig. 12. "Back-calculation" of the matrix flow stress. The fictitious "experimental" composite flow stress has been computed with complex cell arrangement "B", using (a) weak linear hardening, or (b) a Ramberg–Osgood power law as input for the matrix flow stress. From the fictious "experimental" composite flow stress σ_c the matrix flow stress σ_m^{flow} can be derived via Eq. (8). Inserting the RoM, 3pt– or H– values for $E_{\Delta v}$ yields an upper bound for the "back-calculated" matrix flow stress, inserting the 3pt+ or the H+ values yields lower bound solutions. The results are very similar for the other complex cells (A and C).

fraction, V_f, and axial stiffness, E_f, are known, and that the composite stress–strain curve $\sigma_c(\epsilon)$ can be measured with precision, the only unknown remains $\Theta_{\Delta v}$, comprising the stiffness contributions from "constraint" hardening (influence of fibre arrangement) and from "constitutive" hardening (matrix flow stress), the latter being what one aims to measure. We recall again that separation of these two contributions from experimental data is difficult, such that such measurements necessitate either estimates or can only be bounded.

By generating a virtual experimental $\sigma_c(\epsilon)$ curve via FEA (forward analysis) we can now check how different ways of estimating $\Theta_{\Delta v}$ influence the "back-calculated" in situ matrix flow stress (reverse analysis). We focus directly on the elastic–plastic matrix case, as this is the most critical case in this back-calculation problem. Two matrix materials are considered: (i) a matrix with a very low yield strength and a linear hardening rate, as considered throughout this study, and (ii) a (more realistic) Ramberg–Osgood type matrix. The uniaxial matrix flow curves used as input for generating the virtual experimental composite flow curve using complex cell arrangements are shown in Fig. 12, together with the flow curves derived using linear Hill and three-point bounds for $\Theta_{\Delta v}$ ($E_{\Delta v}$) in Eq. (8) for the soft elastic, nearly incompressible material (Table 4). It is seen that the present approach yields useful bounds for the "back-calculated" in situ matrix flow stress, unlike Hill's original incremental lower bound solution. Notably the fairly tight three-point bounds yield very satisfying results for typical (random) composite microstructures, thus showing their usefulness in this task.

Given the performance of these linear three-point bounds, the use of non-linear higher order bounds does not seem justified. Indeed, these are expected to offer only a negligible gain in reducing the bounding interval between the $\Theta_{\Delta v}$ terms. Rather, as shown in what precedes, whatever the bounds used, their spacing is mostly determined by the uncertainty in the extent to which touching fibre rings constrain the matrix. In view of their very cumbersome application in this back-calculation problem, their use does not seem justified.

5. Conclusions

(1) Numerical simulations confirm that Hill's bounds are the best possible general bounds for linear elastic fibrous composites under axial loading, and confirm the validity of three-point bounds for composites with relevant fibre–matrix topologies.

(2) FEA analysis of complex fibre arrangements shows that the main cause for deviations from the rule of mixtures in elastoplastic deformation is

matrix confinement by rings of touching fibres. This effect is clearly visible, but remains fairly limited as long as "realistic" fibre arrangements are considered. Even "artificial" fibre arrangements that maximise this stiffening effect remain more compliant than Hill's upper bound.

(3) Hill's (1964b) extension of his linear bounds to elastic–plastic behaviour of the soft phase seems to use an erroneous value for the shear modulus of this phase. Instead of maintaining its elastic value, as stated by Hill (1964b), it should apparently be given by the common relations between the other (incremental) moduli, while only the bulk modulus preserves its elastic value.

(4) It is suggested that a simple and effective approach to deriving in situ matrix flow curves from composite axial flow curves is by using the elastic three-point bounds, with appropriate phase properties (i.e., non-hardening matrix). This approach, although not fully rigorous, yields very satisfying results when confronted with numerical simulation for Al/Al_2O_3 composites, and provides good precision in the resulting matrix flow curves.

Acknowledgements

This work was funded by core internal funding of the Laboratory for Mechanical Metallurgy at EPFL and by a joint EMPA/EPFL PhD thesis program for one of the authors (BM).

References

Asmani, M., Kermel, C., Leriche, A., Ourak, M., 2001. Influence of porosity on Young's modulus and Poisson's ratio in alumina ceramics. J. Eur. Ceram. Soc. 21, 1081–1086.

Bao, G., Hutchinson, J., McMeeking, R., 1991. Particle reinforcement of ductile matrices against plastic flow and creep. Acta Metall. Mater. 39, 1871–1882.

Benveniste, Y., 1987. A new approach to the application of Mori–Tanaka's theory in composite materials. Mech. Mater. 6, 147–157.

Böhm, H., 1998. COMPCOMP, Rev. A-4LI/137 Institute for Leightweight Structures. Vienna University of Technology, Vienna, Austria.

Böhm, H., Rammerstorfer, F., 1994. Fiber arrangement effects on the microscale stresses of continuously reinforced MMCs. In: Pyrz, R. (Ed.), IUTAM Symposium on Microstructure-Property Interactions in Composite Materials. Kluwer Academic Publishers, Aalborg, Denmark, pp. 51–62.

Böhm, H., Rammerstorfer, F., Weissenbek, E., 1993. Some simple models for micromechanical investigations of fiber arrangement effects in MMCs. Comput. Mater. Sci. 1, 177–194.

Brockenbrough, J., Suresh, S., 1990. Plastic deformation of continuous fiber-reinforced metal–matrix composites: effect of fiber shape and distribution. Scripta Metall. Mater. 24, 325–330.

Brockenbrough, J., Suresh, S., Wienecke, H., 1991. Deformation of metal–matrix composites with continuous fibers: geometrical effects of fiber distribution and shape. Acta Metall. Mater. 39, 735–752.

Buryachenko, V., 1996. The overall elastoplastic behavior of multiphase materials with isotropic components. Acta Mech. 119, 93–117.

Bystricky, P., Bjerregård, H., Mortensen, A., 1999. Plasticity of continuous fiber reinforced aluminum and copper. Metall. Mater. Trans. 30A, 1843–1866.

de Silva, A., Chadwick, G., 1969. Thermal stress in fibre reinforced composites. J. Mech. Phys. Solids 17, 387–403.

Dvorak, G., 1991. Plasticity theories for fibrous composite materials. In: Everett, R., Arsenault, R. (Eds.), Metal Matrix Composites. Mechanisms and Properties. Academic Press, pp. 1–77.

Ebert, L., Hecker, S., Hamilton, C., 1968. The stress–strain behavior of concentric composite cylinders. J. Compos. Mater. 2, 458–476.

Garmong, G., 1974. Elastic–plastic analysis of deformation induced by thermal stress in eutectic composites: I. Theory Metall. Trans. 5, 2183–2190.

Gavazzi, A., Lagoudas, D., 1990. On the numerical evaluation of Eshelby's tensor and its application to elastoplastic fibrous composites. Comput. Mech. 7, 13–19.

Guinovart-Díaz, R., Bravo-Castillero, J., Rodríguez-Ramos, R., Silva, F., 2001. Closed-form expressions for the effective coefficients of fibre-reinforced composite with transversely isotropic constituents. I: Elastic and hexagonal symmetry. J. Mech. Phys. Solids 49, 1445–1462.

Hashin, Z., 1983. Analysis of composite materials—a survey. J. Appl. Mech. 50, 481–505.

Hashin, Z., Rosen, B., 1964. The elastic moduli of fiber-reinforced materials. J. Appl. Mech. 31, 223–232.

Hill, R., 1964a. Theory of mechanical properties of fibre-strengthened materials: I. Elastic behaviour. J. Mech. Phys. Solids 12, 199–212.

Hill, R., 1964b. Theory of mechanical properties of fibre-strengthened materials: II. Inelastic behaviour. J. Mech. Phys. Solids 12, 213–218.

Hill, R., 1965. Theory of mechanical properties of fibre-strengthened materials: III. Self-consistent model. J. Mech. Phys. Solids 13, 189–198.

Hill, R., 1967. The essential structure of constitutive laws for metal composites and polycrystals. J. Mech. Phys. Solids 15, 79–95.

HKS, 1998. ABAQUS/Standard, Version 5.8, User's Manual. Hibbitt, Karlsson & Sorensen, Inc., Pawtucket, RI, USA.

Hu, G., Weng, G., 1998. Influence of thermal residual stresses on the composite macroscopic behavior. Mech. Mater. 27, 229–240.

Huet, C., 1990. Application of variational concepts to size effects in elastic heterogeneous bodies. J. Mech. Phys. Solids 38, 813–841.

Isaacs, J., Mortensen, A., 1992. Structure and room-temperature deformation of alumina fiber-reinforced aluminum. Metall. Trans. 23A, 1207–1219.

Jiang, M., Ostoja-Starzewski, M., Jasiuk, I., 2001. Scale-dependent bounds on effective elastoplastic response of random composites. J. Mech. Phys. Solids 49, 665–673.

Kelly, A., Lilholt, H., 1969. Stress–strain curve of a fibre-reinforced composite. Philos. Mag. 20, 311–328.

Lagoudas, D., Gavazzi, A., 1991. Elastoplastic behavior of metal matrix composites based on incremental plasticity and the Mori–Tanaka averaging scheme. Comput. Mech. 8, 193–203.

Milton, G., 1982. Bounds on the elastic and transport properties of two-component composites. J. Mech. Phys. Solids 30, 177–191.

Mori, T., Tanaka, K., 1973. Average stress in matrix and average elastic energy of materials with misfitting inclusions. Acta Metall. 21, 571–574.

Moser, B., Rossoll, A., Weber, L., Beffort, 0., Mortensen, A., 2001. Nextel™ 610 alumina fibre reinforced aluminium: influence of matrix and process on flow stress. Composites Part A 32, 1067–1075.

Moulinec, H., Suquet, P., 1994. A FFT-based numerical method for computing the mechanical properties of composites from images of their microstructures. In: Pyrz, R. (Ed.), IUTAM Symposium on Microstructure-Property Interactions in Composite Materials. Kluwer Academic Publishers, Aalborg, Denmark, pp. 235–246.

Moulinec, H., Suquet, P., 1998. A numerical method for computing the overall response of nonlinear composites with complex microstructure. Comput. Meth. Appl. Mech. Eng. 157, 69–94.

Mulhern, J., Rogers, T., Spencer, A., 1967. Cyclic extension of an elastic fibre with an elastic–plastic coating. J. Inst. Maths Appl. 3, 21–40.

Nakamura, T., Suresh, S., 1993. Effects of thermal residual stresses and fiber packing on deformation of metal matrix composites. Acta Metall. Mater. 41, 1665–1681.

Ponte Castañeda, P., 1992. New variational principles in plasticity and their application to composite materials. J. Mech. Phys. Solids 40, 1757–1788.

Ponte Castañeda, P., 1996. Exact second-order estimates for the effective mechanical properties of nonlinear composite materials. J. Mech. Phys. Solids 44, 827–862.

Ponte Castañeda, P., 1997. Nonlinear composite materials: effective constitutive behaviour and microstructure evolution. In: Suquet, P. (Ed.), Continuum Micromechanics. IUTAM, Springer Wien New York, Udine, Italy, pp. 131–195.

Ponte Castañeda, P., 2002. Second-order homogenization estimates for non linear composites incorporating field fluctuations: I-theory. J. Mech. Phys. Solids 50, 737–757.

Ponte Castañeda, P., Suquet, P., 1998. Nonlinear composites. In: van der Giessen, E., Wu, T. (Eds.), Adv. Appl. Mech., vol. 34. Academic Press, pp. 171–302.

Qiu, Y., Weng, G., 1992. A theory of plasticity for porous materials and particle-reinforced composites. J. Appl. Mech. 59, 261–268.

Rossoll, A., Moser, B., Mortensen, A., 2003. Longitudinal deformation of fibre reinforced metals: influence of fibre distribution on stiffness and flow stress. Technical report, Ecole Polytechnique Fédérale de Lausanne, Switzerland.

Suquet, P., 1997. Effective properties of nonlinear composites. In: Suquet, P. (Ed.), Continuum Micromechanics. IUTAM, Springer Wien New York, Udine, Italy, pp. 197–264.

Talbot, D., Willis, J., 1997. Bounds of third order for the overall response of nonlinear composites. J. Mech. Phys. Solids 45, 87–111.

Talbot, D., Willis, J., 1998. Upper and lower bounds for the overall response of an elastoplastic composite. Mech. Mater. 28, 1–8.

Tandon, G., Weng, G., 1988. A theory of particle-reinforced plasticity. J. Appl. Mech. 55, 126–135.

Torquato, S., 1991. Random heterogeneous media: microstructure and improved bounds on effective properties. ASME Appl. Mech. Rev. 44, 37–76.

Torquato, S., 1998. Effective stiffness tensors of composite media: II. Applications to isotropic dispersions. J. Mech. Phys. Solids 46, 1411–1440.

Torquato, S., Lado, F., 1992. Improved bounds on the effective elastic moduli of random arrays of cylinders. J. Appl. Mech. 59, 1–6.

Tyson, W., 1975. Discussion of "Elastic–plastic analysis of deformation induced by thermal stress in eutectic composites". Metall. Trans. 6A, 1674–1767.

Wilson, D., Visser, L., 2001. High performance oxide fibers for metal and ceramic composites. Composites Part A 32, 1143–1153.

Yang, S., Gokhale, A., Shan, Z., 2000. Utility of microstructure modeling for simulation of micro-mechanical response of composites containing non-uniformly distributes fibers. Acta Mater. 48, 2307–2322.